sustainability

MDPI

Article

An Approach for Designing Mixed Light-Emitting Diodes to Match Greenhouse Plant Absorption Spectra

Latifa Bachouch [1], Neermalsing Sewraj [2], Pascal Dupuis [2], Laurent Canale [2,*], Georges Zissis [2], Lotfi Bouslimi [1] and Lilia El Amraoui [1]

[1] Research Laboratory Smart Electricity & ICT, SE & ICT Lab., LR18ES44, National Engineering School of Carthage, University of Carthage, 45, Rue des Entrepreneurs, Charguia II, 2035 Tunis, Tunisia; Latifa.Bachouch@enicarthage.rnu.tn (L.B.); lotfi.bouslimi@enicarthage.rnu.tn (L.B.); lilia.elamraoui@enicarthage.rnu.tn (L.E.A.)

[2] LAPLACE, UMR 5213 (CNRS, INPT, UPS), Université de Toulouse, 118 rte de Narbonne, 31062 Toulouse, France; neermalsing.sewraj@laplace.univ-tlse.fr (N.S.); pascal.dupuis@laplace.univ-tlse.fr (P.D.); georges.zissis@laplace.univ-tlse.fr (G.Z.)

* Correspondence: laurent.canale@laplace.univ-tlse.fr

Abstract: We report a methodological approach for simulating luminary output radiation, which is achieved by mixing light-emitting diodes (LEDs) in order to match any plant absorption spectrum. Various recorded narrow-band LED spectra of different colors were first characterized and then fitted with a multi-Gaussian model. An optimizing procedure computed the optimal weighting of the relevant parameters so as to minimize the discrepancy between the combined spectrum and the reference target curve. The particle swarm optimization (PSO) method was applied because it is the most suitable technique for mono-objective situations. Within the useful spectral interval, the worst relative standard deviation between the optimized curve and recorded LED spectral power distribution (SPD) was 3.4%. When combining different LED types, the simulated light output showed that we could limit ourselves to selecting only five colored sources. This work will help us to design an optimized 200 W laboratory luminaire with a pulse-width switched-mode power supply.

Keywords: LED; emission spectrum; optimization; PSO; photosynthesis; McCree

Citation: Bachouch, L.; Sewraj, N.; Dupuis, P.; Canale, L.; Zissis, G.; Bouslimi, L.; El Amraou, L. An Approach for Designing Mixed Light Emitting Diodes to Match Greenhouse Plant Absorption Spectra. *Sustainability* **2021**, *13*, 4329. https://doi.org/10.3390/su13084329

Academic Editors: Lambros T. Doulos, Aris Tsangrassoulis and Umberto Berardi

Received: 7 February 2021
Accepted: 6 April 2021
Published: 13 April 2021

1. Introduction

The light spectrum is a key driver of the photosynthetic processes that are responsible for plant growth, which require about 50% of the waveband of the solar light spectrum that is available in the lower atmosphere [1,2]. Natural light, which extends over the spectral range of 400–1000 nm, is, however, not always available everywhere and at any time in satisfactory quantity and quality. Fortunately, artificial electronic devices have been proven as essential and reliable photon sources for controlled crop lighting and have thereby accelerated the emergence of greenhouses [3–5]. Supplemental lighting has real potential to meet consumers' needs for out-of-season crops with improved yield quality and quantity.

Light-emitting diodes (LEDs) are by far the most promising technology for artificial lighting dedicated to plant cultivation [6,7]. They are mercury-free and combine less radiation loss with an enhanced longevity while affording a good robustness with smaller packaging [8–10]. They entail significant energy savings [11] compared to the less efficient discharge lamps [12,13]. Their recent rapid progress is expected to induce an increase of more than 180% in the horticulture lighting market over the next five years [14].

Over the last 50 years, growth analysis techniques have been widely used to meet the adequate spectra for plants by studying the effects of LED spectra and the photoperiod on the plants' production. Most of them deal only with the McCree target curve, and these are summarized in Table 1. There are also some interesting works that consider LED optimization for the solar spectrum [15,16]. They are beyond our scope, which is only

focused on artificial light for greenhouses. Even if these studies greatly contribute to a better understanding of the interactions between artificial light and the bio-performance of plants, none of them are capable of suggesting a systematic approach to establishing each particular LED combination of a greenhouse LED luminary that is independent of the plant, the target curve, and the desired functionality.

Table 1. Works dealing with optimization of light-emitting diode (LED) light for photosynthesis (Tw: this work).

Ref.	Aim	Plant	Technique
[17]	Optimize output spectrum	Radish and lettuce	Different photon flux density for the circadian cycle
[18]	Crop yield and quality	Lettuce (*Lactuca sativa*)	Coloration, cultivars, and nitrates
[19]	Different seaweed functionalities	Spirulina	Tests with different ratios of red, blue, and green LEDs
[20]	Photosynthesis and photo-pigmentation performance	Different species Non specified	Control of the ratio and shapes of blue and red light, for a multi-package of purplish white LEDs (blue, green, amber, red)
[21]	Different LED photosynthesis photon flux density (PPFD) ratios	Basil	Sensed fluorescent gains as a feedback signal with 4 LEDs
[22]	LED lighting control for plants	Lettuce (*Lactuca sativa*)	Biofeedback control, PPFD values, and adjustment based on a specific threshold of optimal lighting ratios
[23]	Optimize the red–blue combination spectrum	Romaine lettuce	Red and blue light absorbance of lettuce leaves
[24]	Maximize efficiency of crop production	Chinese cabbage	Estimation of crop yield following the light regime
[25]	Optimize the LED combination	Cucumber	PSO to evaluate the numer of operating LEDs
[26]	Optimize LED spectrum	Ornamental plants	Lighting tests, and a visual assessment survey for various light system hypothesis using different peak wavelengths
[27]	Optimize the LED spectrum	Lettuces and other green plants	Red, blue, and green LEDs. Light efficiency and PPFD level determined by maximizing the similarity between the LED spectrum and the McCree curve.
Tw	Optimize the LED spectrum	None	Three luminaries involving 9 LEDs to match the McCree curve

McCree [28] and then Inada [29] conducted pioneer studies to evaluate the frequency dependency of the efficiency of photosynthetic activity. In 1972, McCree measured the action spectra for 22 species of crop plants and concluded that all the action spectrum curves follow a similar shape. His approach was based on the adjustment of the irradiance level at different wavelengths, producing a constant photosynthetic rate, without mentioning the spectral exit width or the irradiance. In addition, different metrics were used. His results are not easily reproducible [28]. According to a recent work by Wu et al. [30], there exist many contradictions concerning the different target curves of McCree, who carried out measurements with optical filters or monochromators. Moreover, different values of the full width at half maximum (FWHM), quantification strategies, and metrics lead

to different curve shapes. These considerations can lead to misinterpretation of spectral response data.

In the field of plant study, it is considered that light is used in the Photosynthetically Active Radiation (PAR) band, which corresponds to the 400–700 nm range. Only a fraction of the photons arriving on a plant surface can be used for photosynthesis: measurements characterize either the external photons flux or their internal use expressed as internal relative quantum efficiency. Plant light quantification uses three main approaches, namely the Photosynthetic Photon Flux (*PPF*), the Yield Photon Flux (*YPF*), and the energy Flux [31]. The ratio between the *PPF* and the *YPF* is given by the action spectrum. Some authors consider the amount of photons to be important; others consider their energy to be the driving variable. There is no official SI unit for photon flux density measurement *PPFD*. Thus, in Equation (1), a mole of photons is used to designate Avogadro's number (N_A = 6.022 141 $\cdot 10^{23}$ mol^{-1}) of photons for stoichiometry [32,33]. The unit $\mu mol \cdot m^{-2} \cdot s^{-1}$ is most suitable for *PPF*, since it accounts for the number of photons in the *PAR* spectral range [34,35]. It can be considered as the production efficiency of C_3 maximizing photosynthesis. In our study, we considered the target curve in relative units. Its shape is sufficient to perform optimization to meet the target curve for photosynthesis, the concept of which is related to both the emitting source radiation power and the light received by the plants. It is a photochemical reaction within the chloroplasts of plant cells in which light energy transforms atmospheric carbon dioxide (CO_2) into carbohydrates [13]. We consider the photosynthesis C_3 process, which involves CO_2, ribulose-1,5-bisphosphate ($C_5H_{12}O_{11}P_2$), and phosphoglyceric acid ($C_3H_7O_7P$) containing, respectively, 1, 5, and 3 carbon atoms, according to Equation (1) [36].

$$C_5H_{12}O_{11}P_2 + CO_2 + H_2O + \text{Photons} \longrightarrow 2\,C_3H_7O_7P \quad (1)$$

Photosynthesis processes involve various pigments such as chlorophyll a, chlorophyll b, and carotenoid [37]. Plants mainly require certain specific radiations [38–41], mostly concentrated in the red and blue regions [42–46]. Therefore, artificial light should be adjusted to match individual plant target spectrums. Broadband artificial light sources are less efficient due to unused radiation. On the contrary, *LEDs* are suitable artificial sources due to their single narrow emissions (spectral widths in the range 15–30 nm). About 20 different *LEDs* are required to cover the solar visible range. However, following specific photosynthesis processes, any plant may require at most 10 different *LED* types.

On the other hand, it is interesting to reduce the number of different *LED* types in an industrial setting. Even if this increases the deviation of the simulated curve compared to the target one, it induces only a slight loss in energy efficiency (about 5 % [47]). However, the benefits are numerous: reduction in production cost, simpler driver electronics, increased reliability, and reduced maintenance cost [47,48]. This is why we lowered the number of *LED* types to 5 different colored *LEDs* while maintaining the same overall electrical power injected into the LEDs.

Our *LED*-type optimization technique is performed stepwise, as follows. In a first approach, we started by mixing three useful emissions from red (R_1), green (G), and blue (B_1) *LEDs*. In a second step, we added the wide middle-band white (W) *LED* to account for more middle range photons, which are also useful for photosynthesis. This combination was finally upgraded, in a third step, by adding 2 red (R_2 & R_3), 1 blue (B_2), 1 yellow (Y), and 1 amber (A) additional *LEDs*. The important blue and red wings as well as the useful middle-range light were thus well represented. In a second approach, we limited ourselves to only 5 colored *LEDs*, offering only narrow emissions. We selected the R_1, R_2, G, A, and B_2 *LEDs* that enhance photosynthesis processes. The peak emissions of the colored *LEDs* were 450 nm (deep blue: B_2), 460 nm (blue: B_1), 527 nm (green: G), 590 nm (amber: A), 610 nm (yellow: Y), 630 nm (red: R_1), 660 nm (deep red: R_2), and 680 nm (far deep red: R_3).

The present work is thus dedicated to a methodological approach that can be adopted to optimize any *LED* lighting situation, provided that the target spectrum is available. We chose the most commonly used *McCree* target curve in relative units.

The paper is organized as follows. The next section very briefly presents the materials and methods used. Our experimental results and simulation calculations are discussed in Section 3, before concluding and suggesting our future built-in switched-mode power supply and *LED* luminary.

2. Materials and Methods

2.1. LEDs *Characterization*

The opto-electrical setup illustrated in Figure 1 was used to measure each *LED* spectrum within 380 and 780 nm together with its electrical characteristics.

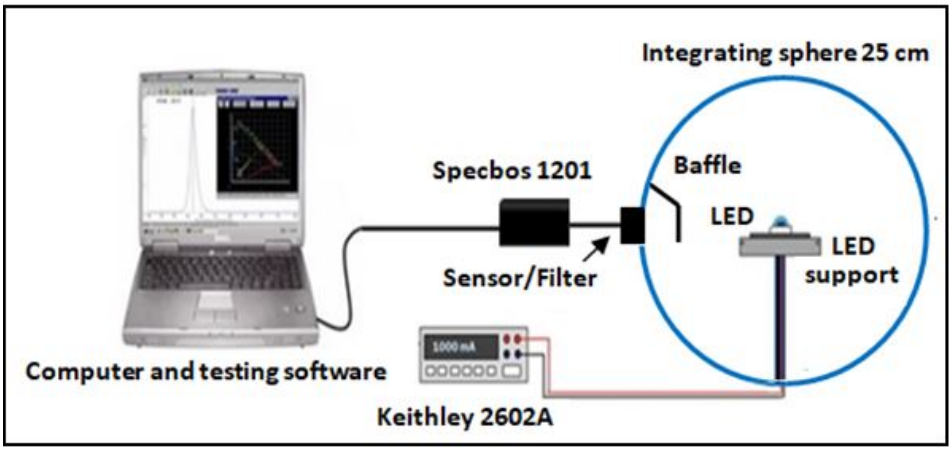

Figure 1. Light-emitting diode (LED) electrical and optical measuring device.

There exists a large number of *LED* manufacturers such as Osram, Cree, Osram Golden Dragon, Multicomp Pro, Bridgelux, Philips, etc. High-power *LEDs* are selected due to their high luminous efficiency. The different *LEDs* selected for this work are as follows:

- Multicomp Pro *THEM-CLRX* for R_1-630 nm [49], *THEM-CLGX*(*520535*) for *G*-527 nm [50], *THEM-CLAX* for A-590 nm [51], and *THEM-CLBX 460-470* for B_1-460 nm [52];
- Osram *LD W5SM* for B_2-450 nm [53], OSLONSSL 150 for R_2-660 nm [54], Golden Dragon *LH W5AM* for R_3-680 nm [55], and *LA W5AM* for *Y*-610 nm [56];
- Bridgelux: *ES Star Arrays, BXRA-27E0540-A-03* (Warm) for the white *LED* [57].

The *LED* electric and optical parameters are the forward current, forward voltage, peak wavelength λ_p, and full width at half maximum (*FWHM*) $\Delta\lambda$. The constructor's values are given in Table 2. For the narrowband *LEDs*, $\Delta\lambda$ ranges between 18 and 41 nm. The white *LED* used for this work is seen as an entity, even if in fact it comprises several serial *LEDs*. Its forward voltage is much higher than our colored *LED* ones.

Table 2. Electric and optical *LED* parameters: constructor's values.

LED Type	I_{nom} (mA)	V_F, typ. (V)	λ_p(nm) Min	λ_p(nm) Max	$\Delta\lambda$ (nm)
Deep blue (B_2)	350	3.2	449	455	25
Blue (B_1)	350	3.2	460	470	27
Green (*G*)	350	3.4	520	535	41
Amber (*A*)	350	2.2	585	595	18
Yellow (*Y*)	400	2.3	612	616	18
Red (R_1)	350	2.2	620	630	18
Deep red (R_2)	350	2.1	646	666	18
Hyper red (R_3)	400	2.2	660	666	25
White (*W*)	350	18.2	—	—	—

2.2. SPD Measuring Device

A tunable pulsed current source (*Keithley 2602A*) can supply the *LED* circuit up to 1 A via a *DC* voltage, which can attain 40 V. The *Keithley* current source provides an accurate pulse current, bringing together the supply and the digital multi-meter in a single device. Each *LED* (device under test) is successively placed at the center of an optical 25 cm diameter *Ulbritch* integrating sphere (*LabSphere* 1 000) equipped with a spectro-photo-radiometer (*Specbos* 1 201) operating in radiance mode and targeting one of the internal shields. The values reported in Table 3 are the maximum spectral flux densities as well as the total fluxes. The integrated value of the *SPD* of the white *LED* is determined by integration on the plant spectrum 400–700 nm. The sphere form factor was not established, but it can safely be assumed that it stays constant amongst all the measurements. For this reason, the *LED* output light level is reported as "relative value". The design factor taken into consideration in order to optimize the amount of *LEDs* of different colors is the ratio of radiometric power densities.

The emitting *SPD* of each *LED* is carried out at the same mean pulsed current of 20 mA, with a duty cycle of 10% at a pulse repetition rate of 1 kHz, corresponding to a peak current of 200 mA. We limited our measurements to such a low average current and short duty cycle to prevent excessive heating of the *LEDs* in the closed and non-ventilated integrating sphere. At this current value, heating effects are acceptable and the *LED* emissions suffer no significant degradation. Therefore, for the present study, we can use a simple mathematical modeling for our colored *LEDs*.

2.3. Modeling Colored LEDs

An accurate evaluation of individual *LED SPDs* constitutes an important step to evaluate parameters of the combined *LEDs* such as luminous flux, chromaticity, color quality, as well as many other parameters [58–60].

This approach is essential for a new design methodology for lighting applications with narrowband emissions and fast electrical modulability.

Until now, there have been three main approaches including a purely mathematical approach, combined approach between mathematical descriptions and *SPD* measurements, and finally a more physical one.

At the beginning, in 2000, the first attempt for modeling *LED SPDs* was proven to be rather simple and non-satisfactory [61]. Since about 2005, several publications appeared, where their radiation modeling were constantly improved. The single Gaussian fitting [62] remains non-satisfactory because of the asymmetry of the emission. It was afterwards enhanced with a double Gaussian model [63–65], which nowadays, is still widely used by many authors and organizations. However, both the current and temperature dependence of the *LED's* spectrum are not accounted for by this approach. In 2008, Chou et al. [66] reported a variant of the split Gaussian function with different exponential behaviors on either side of the peak emission.

In 2010, F. Reifegerste and J. Lienig [67] undertook a thorough and deep investigation modeling in order to evaluate several single-colored *LED* spectra. Since then, they have significantly improve their models when dealing with the design of multi spectral *LED*-based illumination systems. In a first step [68,69], they focused mainly on the selection of *LEDs* for an aimed spectrum from a database of measured LED devices. They also considered efficient mixing of the light from different *LEDs* as well as the final control of the spectra in a particular application [70].

All these above models were solely mathematical without any link to underlying physical principles. However, due to the large number of fitting parameters of these mathematical models developed during the last decade, an easy-to-use modeling approach could not be provided.

In 2010, Keppens et al. [71] reported a spectrum model, constructed with a Boltzmann exponential behavior and accounting for carrier temperature variation, gap band energy shift, as well as the increase in the non-radiative recombination rate with junction tempera-

ture. Even if this model allows for very accurate simulations of single-color *LED* spectra (like ours), in real operating conditions, it remains too cumbersome for integration with our present optimization process of *LED SPDs*.

For our purpose, mathematical models are much more relevant, particularly when we do not account for junction temperature variations, such as in the present study. Therefore, among the several mathematical functions listed by Vinh et al. [72] now available for curve-fitting of *LED SPD*, namely the second-order Lorentz, Pearson VII, Split Pearson VII, Gaussian, Split Gaussian, multi-Gaussian, etc., we retained the latter. Indeed, thus far, it is the best mathematical approach because of its non-symmetry and its simplicity.

For each *LED*, the mathematical single-Gaussian function of the *SPD* is given by the following expression:

$$S_\lambda(\lambda, \lambda_p, \Delta\lambda) = S_p \cdot e^{-(\frac{\lambda-\lambda_p}{\Delta\lambda})^2} \quad (2)$$

with
$0 \ll S_p \ll 1$, $\lambda_p \in [380, 780]$ nm and $\Delta\lambda \in [10, 30]$ nm

The multi-Gaussian model is expressed as follows:

$$S_\lambda(\lambda) = \sum_i S_{pi} \cdot e^{-(\frac{\lambda-\lambda_{pi}}{\Delta\lambda_i})^2}, \quad (3)$$

where i denotes the ith Gaussian term. The optimal number of terms is determined by the correlation indexes R^2 and R^2_{adj} given by Equations (4) and (5), as explained in [73]:

$$R^2 = 1 - \frac{\sum (S_\lambda(\lambda) - S_{T,\lambda}(\lambda))^2}{S_\lambda(\lambda)^2 - \frac{(\sum S_\lambda(\lambda))^2}{n}}, \quad (4)$$

$$R^2_{adj} = 1 - (1 - R^2)\frac{n-1}{n-p-1}, \quad (5)$$

where n is the number of recorded samples in the wavelength range, p is the total number of explanatory variables, $S_{T,\lambda}(\lambda)$ is the measured *LED* spectrum, and $S_\lambda(\lambda)$ is the simulated one. The model order was selected by maximizing the R^2_{adj} indicator, which permits us to apply a parsimony principle: higher-order models with modest improvement in error reduction are penalized.

2.4. Optimization Approach

In order to match the target spectrum with our calculated one (obtained via an optimized set of our individual *LED*'s *SPD*), the adopted optimization procedure is carried out as follows. The fitted spectrum is obtained by compounding the multi-Gaussian formulation of the relevant *LED* spectra. Our optimization is based on minimization of the error between the compound *LED* spectrum and the target spectrum of the plants by using a single objective optimization procedure. In this case, *PSO* is fully suited.

We denote by X a vector containing the variable parameters:

$$X = [X_1, X_2, \ldots X_k, \ldots], \quad (6)$$

where X_k is the weighted factor of the kth *LED* (noted k-type *LED*, i.e., B_2, B_1, G, A, Y, R_1, R_2, R_3, W, or B_2, G, A, R_1, R_2) and the *LED* drive current. These coefficients are very important for *LED* spectra optimization. The simulated spectral power distribution of plants $S_\lambda(\lambda)$ is given by the following mathematical model:

$$S_\lambda(\lambda) = \sum X_k \cdot S_{k,\lambda}(\lambda), \quad (7)$$

where $X_k = a_k \times n_k$ is the corrected quantity of the k-type *LED*, n_k is the quantity of the k-type *LED*, a_k is the transfer coefficient between the spectral radiant intensity and the

LED's drive current, and $S_{k,\lambda}(\lambda)$ is the simulated *SPD* spectrum of the k-type *LED*. The spectral power distribution $S_{T,\lambda}(\lambda)$ is a relative spectrum.

The fitting accuracy depends on the *LED*'s *SPD* and the number of *LED*s. The optimal *LED* spectrum is achieved by searching the optimal *LED*s number. The relative weighting parameter X_k, of the corresponding light source is obtained by maximizing the likelihood between the objective target spectrum and the generated one (*LED SPD*). The best *LED* spectrum fitting is performed using the correlation index R^2 as the fitting parameter, as explained in the previous section. The objective function used to minimize the error is given by the following expression:

$$min(\sum (S_\lambda(\lambda) - S_T(\lambda)^2)), \tag{8}$$

subject to the constraints set

$$\Omega = \{b_{XL} \ll X \ll b_{XH}\}. \tag{9}$$

In these expressions, the lower bound vector, b_{XL}, equal to 1, and the upper bound vector, b_{XH}, equal to 200, are the design variables defining the search range. The *PSO* technique will be described in full details in the next subsection.

2.5. Optimization Program: Particle Swarm Optimization Method

Kennedy and Eberhart [74] mutually developed the *PSO* process in 1995. The algorithm was inspired by the behavior of birds inside flocks, each bird at a position x searching for food with a velocity v, where the individuals look for the best individual and swarm solution in a problem dimensional space. This method searches the optimal solution using a population of particles, defined by their respective individual positions and velocities, in the search space, which is, in our case, the weighted number of *LEDs*.

This way, each individual particle, denoted as I, is characterized by its current position x_i, its current velocity v_i, and its best current position P_{besti} (the position in the parameter space of the best fit returned for a specific particle) in the search space. The corresponding position in the parameter space of the best fit returned for the entire swarm g_{besti} is also simultaneously calculated.

The position and the velocity of the particles are modified and adjusted according to the communication between the different particles of the swarm. The individual particles update their position, velocity, and P_{best} as well as the swarm position set by searching for a new position x_i, velocity v_i, P_{besti}, and g_{besti} set and by comparing it to the previous one.

Through successive iterations, we converge to the optimal solution. The particles are represented in a D-dimensional space as follows:

$$x_i = (x_{i,1}, x_{i,2}, \ldots, x_{i,D}), \quad v_i = (v_{i,1}, v_{i,2}, \ldots, v_{i,D})$$
$$P_{besti} = (P_{besti,1}, P_{besti,2}, \ldots, P_{besti,D}).$$

Assuming that each individual set of x_i, v_i, P_{besti}, and g_{besti} is known at time iteration k, the new set, at time iteration $(k+1)$, is calculated according to the following equations:

$$v_i^{k+1} = \omega(k) \cdot v_i^k + c_1 \cdot rand[] \cdot (P_{besti} - x_i^k) + c_2 \cdot rand[] \cdot (g_{besti} - x_i^k) \tag{10}$$
$$x_i^{k+1} = x_i^k + v_i^{k+1}; \quad k = (1, 2, \ldots, N) \tag{11}$$
$$\omega(k) = \omega_{max} - (\omega_{max} - \omega_{min}) \cdot \frac{k}{k_{max}} \tag{12}$$

where c_1 and c_2 are acceleration values, which determine how fast a *PSO* particle moves towards P_{besti} and g_{besti}. The term $\omega(k)$ is the inertia weight, which influences the convergence behavior of *PSO*. It evolves linearly over iterations, with the initial and final values being noted ω_{max} and ω_{min}. The maximum time iteration number is controlled by k_{max}.

In this mono-objective *PSO*, each *LED*-type is considered a swarm-particle. The number of a particular colored *LED* represents its position (at iteration k). A set of random numbers gives the progression speeds of all the particles, which allows for the calculation of the new position (iteration $k+1$). Optimization is achieved by considering the whole spectral domain at a time by using Equation (12). The different steps of the optimization procedure are depicted by the flowchart given in Figure 2.

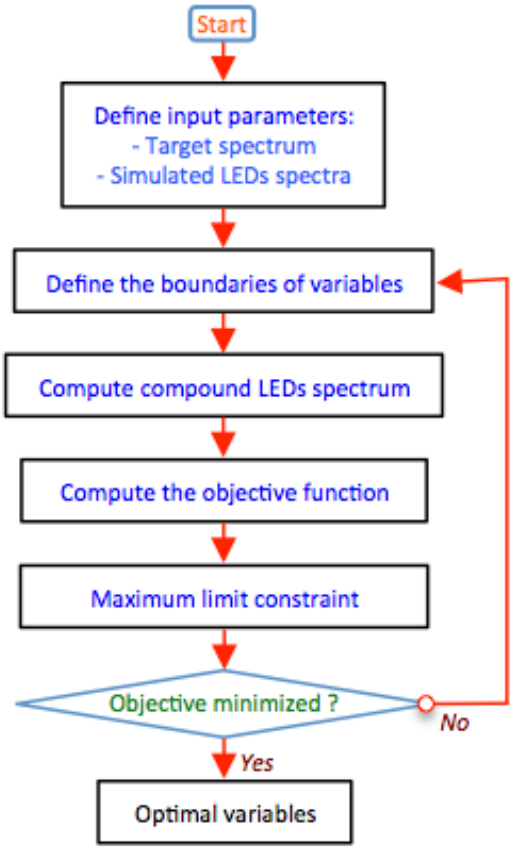

Figure 2. Flowchart of the particle swarm optimization method.

3. Results and Discussions

3.1. Modeling Light Distribution of Monochromatic LED

For each *LED*, our results follow a similar pattern. For instance, the mean forward voltage of the B_1 *LED* is 2.7 V (Table 3). It is about 20% less than the constructor's values (Table 2). Such a discrepancy results typically from the parameter spread of electronics devices.

The recorded spectrum of the B_1 *LED* is depicted in Figure 3b, while its peak wavelength, *FWHM* as well as forward voltage are given in Table 3. The B_1 *SPD* is non-symmetric (crosses: measured spectrum, full line: Gaussian sum fit). The fit is very good as confirmed by Table 4 ($R^2_{adj} = 0.9993$ for B_1), where all the fitting parameters are given for all the colored *LEDs*. Their *SPDs* are given in Figures 3 and 4. R_3's *SPD* (3 exponential terms), which is very similar to that of R_2 (3 exponential terms, as well), which is not given. These results comfort our idea of retaining the multi-Gaussian model. Three or four exponential terms are required for our colored *LEDs*. Figure 3d represents the measured and simulated values of the *W* white *LED*'s *SPD*, which cannot be modeled with a Gaussian sum.

The measured peak wavelengths, *FWHM* together with the *LED* forward voltages for all the *LEDs* are given in Table 3. The optical values sometimes differ from the constructor's ones, most likely because the substrate of a same *LED* sample is not reproducible and because heating effects lead to a shift in the peak emission [75].

Correlation index R^2 is estimated on the whole spectral domain from 380 to 780 nm. For each *LED*, deviations occurring far from the *LED* spectral range (and in the wings

of the emission) do not affect the optimization performance. Therefore, we also estimate the difference between the fitted values and the recorded ones, only in the useful spectral interval corresponding to the *FWHM* of each recorded *SPD*. For this domain, we calculate the standard deviation of our fitted curves. This standard deviation remains quite low, within 3.4 % and 0.68 % of each peak *SPD* value S_p (Table 3). The worst situation occurs for the R_1 *LED*. In order to further appreciate the curve fitting impact on optimization, we also calculate the difference between the experimental and fitted values in this domain. The specific wavelength λ_e corresponds to the worst situation for which the absolute difference is the highest. The relative difference is reported in Table 3. This local error varies between 1.1% and 3.8%, the most unfavorable situation occurring for the amber *LED*. Nevertheless, a close look at all these *SPDs* (Figures 3 and 4) clearly shows that our experimental curves are well described by the multi-Gaussian fitting curve.

Table 3. Measured electric and optical *LED* parameters, and fitting parameters at 20 mA (σ is the standard deviation, and percentage values with respect to peak value are given in parenthesis).

LED Type	V_F (V)	λ_{peak} (nm)	$\frac{\Delta\lambda}{2}$ (nm)	S_p (a.u.)	σ (%) (a.u.)	Error at λ_e (%)	λ_e (nm)	Integrated Value of *SPD* (a.u.)
B_2	2.56	447	9.5	16.04	0.435 (2.7 %)	0.325	447	0.558
B_1	2.70	468	9	16.94	0.475 (2.8 %)	1.96	470	0.404
G	2.69	527	13	7.76	0.173 (2.2 %)	2.73	537	0.168
A	1.74	591	7	23.43	0.160 (0.68 %)	3.79	587	0.085
Y	1.76	604	7	14.23	0.311 (2.2 %)	1.05	597	0.170
R_1	1.73	628	7.5	12.00	0.409 (3.4 %)	1.67	621	0.234
R_2	1.68	657	6.5	11.36	0.366 (3.2 %)	2.09	662	0.198
R_3	1.76	679	6.5	21.07	0.702 (3.3 %)	1.47	676	0.392
W	14.4	610	—	15.98	—	—	—	2.47

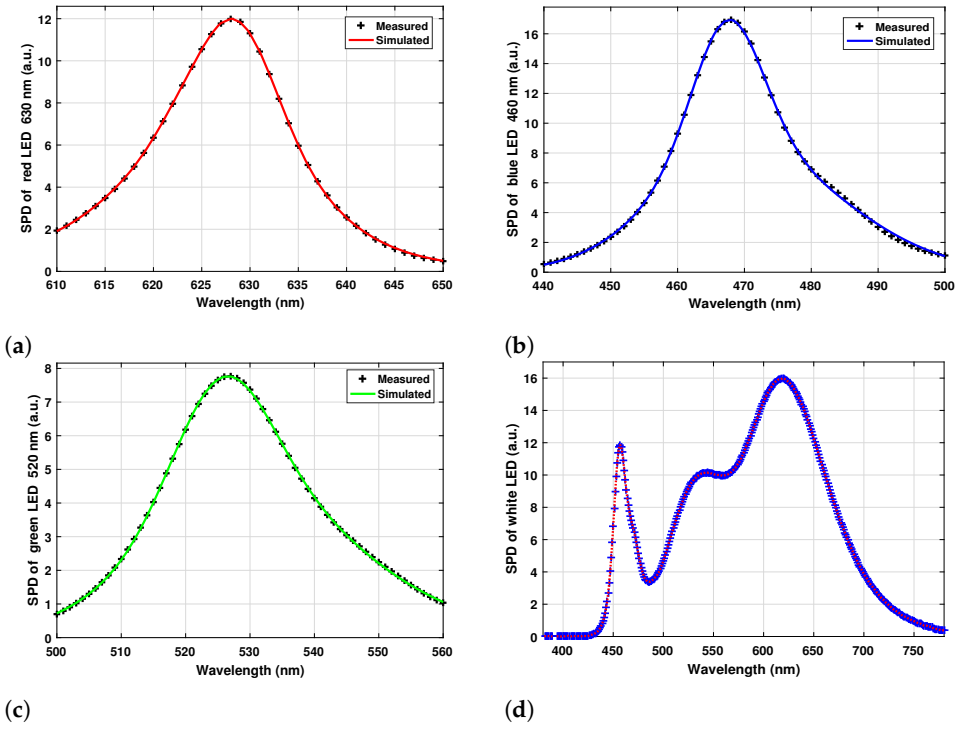

Figure 3. Measured and simulated *LED SPDs* at 20 mA: (**a**) R_1 *LED*; (**b**) B_1 *LED*; (**c**) *G LED*; (**d**) White *LED*.

Table 4. *SPD* multi-term Gaussian fitting parameters of the different *LEDs*.

LED Type	Term Nº	S_{pi} (a.u.)	λ_{pi} (nm)	$\Delta\lambda_i$ (nm)
Deep blue B_2 450 nm R^2_{adj} = 0.9997	1	10.5	446.1	7.4
	2	[10.3, 10.6] 2.16	[446, 446.2] 457.6	[7.3, 7.5] 25.5
	3	[2.00, 2.33] 12.0	[457.1, 458.2] 449.0	[25.1, 25.8] 15.1
		[11.9, 12.2]	[448.9, 449.0]	[14.9, 15.2]
Blue B_1 460 nm R^2_{adj} = 0.9993	1	8.84	467.2	7.2
	2	[8.50, 9.17] 8.47	[467.1, 467.3] 470.3	[7.0, 7.3] 19.8
	3	[8.05, 8.88] 0.64	[469.3, 471.3] 453.8	[19.3, 20.4] 8.9
		[0.59, 0.69]	[453.2, 454.4]	[8.6, 9.2]
Green G 527 nm R^2_{adj} = 0.9993	1	4.99	526.5	15.1
	2	[4.90, 5.07] 1.02	[526.1, 526.9] 550.8	[14.7, 15.4] 15.0
		[0.93, 1.10]	[549, 552.6]	[13.5, 16.6]
Amber A 590 nm R^2_{adj} = 0.9997	1	3.63	591.0	4.1
	2	[2.78, 4.47] 2.35	[590.7, 591.3] 585.0	[3.8, 4.6] 5.0
	3	[1.78, 2.91] 1.91	[584.2, 585.8] 597.0	[4.2, 5.9] 6.2
	4	[1.70, 2.12] 0.88	[596.1, 597.9] 577.0	[5.7, 6.8] 8.1
		[0.73, 1.03]	[575.1, 578.0]	[6.9, 9.3]
Yellow Y 604 nm R^2_{adj} = 0.9999	1	38.0	604.1	5.0
	2	[37.3, 38.7] 44.9	[604, 604.2] 602.1	[5.0, 5.1] 10.5
	3	[44.3, 45.5] 14.6	[602.0, 602.2] 598.6	[10.4, 10.7] 19.4
		[13.8, 15.4]	[598.4, 598.7]	[19.2, 19.7]
Red R_1 630 nm R^2_{adj} = 0.9997	1	1.81	628.2	4.5
	2	[1.20, 2.43] 0.37	[628.1, 628.4] 612.8	[3.9, 5.1] 4.3
	3	[0.28, 0.46] 7.74	[612.2, 613.5] 627.6	[3.4, 5.2] 8.9
	4	[7.18, 8.31] 2.55	[627.5, 627.7] 624.3	[8.5, 9.3] 20.6
		[2.33, 2.78]	[624, 624.5]	[20.0, 21.2]
Deep red 660 nm R^2_{adj} = 0.9993	1	8.88	657.1	5.73
	2	[8.83, 8.93] 2.2	[657, 657.2] 647.9	[5.69, 5.78] 5.35
	3	[2.14, 2.27] 2.53	[647.8, 648.1] 649.6	[5.18, 5.51] 19.3
		[2.48, 2.59]	[649.5, 649.7]	[19.1, 19.4]
Hyper red R_3 680 nm R^2_{adj} = 0.9994	1	15.8	678.9	5.76
	2	[15.7, 15.9] 2.93	[678.9, 679] 669	[5.72, 5.80] 6.13
	3	[2.81, 3.04] 5.67	[668.7, 669.2] 671	[5.87, 6.40] 19.5
		[5.56, 5.78]	[670.9, 671.1]	[19.3, 19.6]

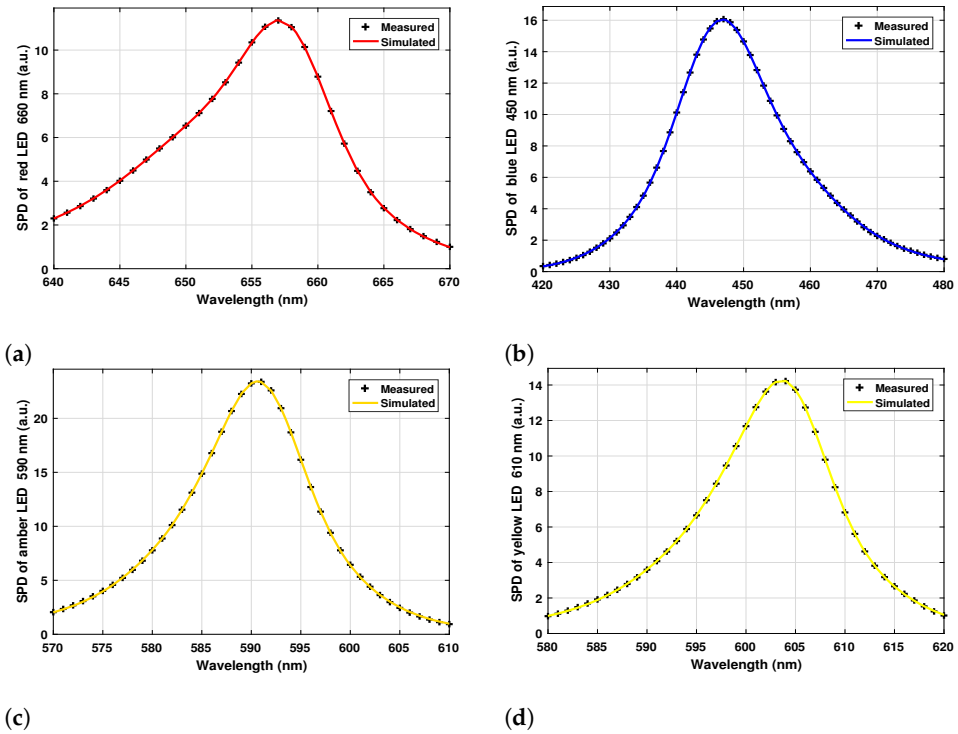

Figure 4. Measured and simulated *LED SPDs* at 20 mA: (**a**) R_2 *LED*; (**b**) B_2 *LED*; (**c**) *A LED*; (**d**) *Y LED*.

3.2. Combining 3, or 4, or 9 Selected LEDs

Mixed *LED* output light optimization is firstly performed with the simplest and basic combination involving only three *LEDs* and depicted in Figure 5a with the blue dashed curve. The red and blue *LEDs* can provide only some of the required radiations for photosynthesis, while the green *LED* alone cannot meet our objective for the middle region of the spectrum. The four *LED*-type optimized spectrum (represented by the green curve) better fits the target curve. Finally, using all the nine *LEDs*, the simulated spectrum (blue full line curve) is much enhanced. Of course, the B_2, R_2, and R_3 *LEDs* and to a lesser extent the *A*, *Y*, and *G* ones improve the output emission. The amount of R_1, B_1, and *G LEDs* hardly varies for the three combinations due to the nonoverlap of their respective individual sharp emissions (Table 5). The correlation index between the target curve and the simulated one is equal to 0.33, 0.44, and 0.87 for R_1GB_1, R_1GB_1W, and all the nine *LED* combinations, respectively. As expected, the amount of R_1, B_1, and *G LEDs* hardly varies for the three combinations (Table 5).

The total number (summing up the individual *LED* amounts) of *LEDs* needed for the R_1GB_1, R_1GB_1W, and $R_1GB_1WR_2R_3YB_2A$ luminaires are 291, 355, and 752, respectively. For the three luminaires, the number of individual R_1 (B_1 and *G* as well) *LEDs* is hardly affected due to nonoverlap of the individual *LED SPDs*. We point out that attention should not be paid to these absolute values but instead to the relative ones. These values will differ following the target curve. Such high amounts of *LEDs* may increase the thermal and screening effects. As explained earlier, it can also be an issue for driving and control with switched-mode power *LED* drivers. To minimize these effects, the overall luminaire power should be distributed over a number of *LED* heat-sinks, each supporting only a limited amount of *LEDs*.

Table 5. *LED* amounts for different combinations.

		LED Type									Total *LED*
	#	B_2	B_1	G	A	Y	R_1	R_2	R_3	W	Amount
PAR McCree	3		49	151			91				291
	4		51	151			92			61	355
	9	49	50	152	189	40	92	82	38	60	752

#: number of *LEDs* in the *LED* combination (luminary); #3: R_1GB_1; #4: R_1GB_1W; and #9: All 9 *LEDs*.

3.3. *Combining Only 5 Selected* LEDs

The simulation results, obtained with 5 *LEDs*, are shown in Figure 5b. The correlation index between the *McCree* target spectrum and the generated one is equal to 0.73. Table 6 represents the best percentage of each *LED* type. We give the required distribution of different *LEDs* (5-LED mix) to match the *McCree* spectrum.

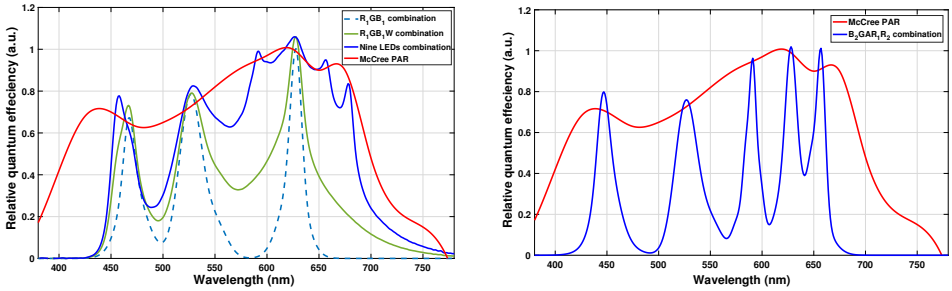

(**a**) (**b**)

Figure 5. Different *LED* combinations: (**a**) 3-, 4- and 9-*LED* mixing spectrum optimization and (**b**) 5-*LED* mixing spectrum.

Table 6. Weight values and relative power density for each *LED* type.

LED Type	*LED* Nb	*McCree* Coeff.	%	Relative Power Density %
B_2	20	$X_1 = 49$	8.7	18.4
G	26	$X_2 = 150$	26.7	24.0
A	25	$X_3 = 189$	33.7	15.5
R_1	28	$X_4 = 84$	15.0	19.6
R_2	29	$X_5 = 89$	15.9	17.8

3.4. *Designing a Future Experimental 200 W Target* LED *Lighting System*

Based on the above optimization procedure, we are currently designing an experimental 200 W target *LED* luminary adopting four 50 W serial devices in order to minimize the heat effects of the neighboring *LEDs*. Our device is based on high power surface-mounted *LEDs* (*SMD*). These versatile lighting sources comprise individual *LEDs* operating around at least 1 W. *SMD LEDs* are usually equipped with a lens permitting to control the main emission lobe aperture. This way, matching source and receptor does not require an external part. Therefore, this specific feature can provide strong emitted radiations for plants while reducing wasted light and energy. In order to irradiate plants grown on a target area, a uniform light distribution is needed.

We supply each *LED* with 280 mA in order to determine the amount of *LEDs* required for each family. This current value results from the 200 W *LED* luminary target-power of our future Buck power supply, which is limited to an output current of 1.4 A, according to a former survey work performed at the EI & ICT ENICarthage laboratory [76–78]. The

corresponding supply output voltage is 143 V. We need to verify that this new current value does not bring any significant drift on the target spectrum.

4. Conclusions and Perspectives

In this paper, a *LED* luminary output radiation is simulated from individual recorded *LED SPDs* to achieve the optimal output spectrum for greenhouse plants. The mono-objective *PSO* technique is applied to match the target spectra. This simple optimization approach of *LED* luminary radiation can be easily used for any particular target application, provided that the latter is reliable. Despite their importance for photosynthesis, altogether blue and red wings are insufficient to irradiate all types of plants. In this work, a limited amount of prominent *SMD LED* mixing, covering also the middle region, was proven to approach the target spectrum.

For our next work, we are designing a new experimental *LED* luminary using a *COMSOL* multiphysics environment while accounting for thermal processes. We conceived the printed circuit board (*PCB*) using Altium Designer. Using a buck driving supply, we will provide dimming control in order to adjust the adequate spectrum to meet the needs of the plant. The supply is configured with multi-*LED* strings using constant current control, which accounts for a tradeoff optimization between electric power losses and volume minimizations in order to achieve higher efficiency and better reliability. We plan to record the target *PAR* adapted to the specific studied plant. Then only, field studies will permit us to analyze the physiological effects of our optimized lighting system, using a dimming based on pulse width modulation (*PWM*) control in order to provide the optimal light quantity and quality throughout the different growth phases of the selected plants under study.

Author Contributions: This work was conceptualized by P.D., L.B. (Latifa Bachouch), G.Z., and N.S. The numerical code was written by both L.B. (Latifa Bachouch) and P.D.; N.S. helped in building the MatLAB program. The PSO technique was implemented by L.B.(Latifa Bachouch), who also performed all the experiments. She was trained by P.D. for the experimental setup as well as by N.S. for the handling of monochromators and optical measurements. The article was written by L.B. (Latifa Bachouch) with contributions of N.S., P.D., and L.C. The latter greatly contributed to *LED* selection and designed the *LED* support. The results were analyzed by L.B. (Latifa Bachouch), N.S., and P.D. All the authors participated in the follow-up of this work. All authors have read and agreed to the published version of the manuscript.

Funding: This work was supported by LAPLACE Light & Matter Team equity financing. The three-months stay of L.Bh. in Toulouse was supported by the Carthage University Scholarship 2018-BALT-958 with the precious help of Lotfi Bouslimi and Lilia El Amraoui.

Institutional Review Board Statement: Not applicable.

Informed Consent Statement: Not applicable.

Data Availability Statement: Not applicable.

Acknowledgments: L.B. (Latifa Bachouch) is very grateful to the LM–Team, the Electronic service, and the LAPLACE Laboratory for providing the facilities to carry out this work within the three months of her internship in Toulouse. She is also very grateful to Frank Reifegerste for useful discussions concerning *LED* modelling. She also is very grateful to her supervisors of SE & ICT Lab., namely Lilia El Amraoui and Lotfi Bouslimi, for their follow-up and contribution to this work. She would also like to thank the following Bachelor students of the University of Toulouse who helped in the bibliographic work: Léa Dubaèle, Léa Leblanc, Arthur Galand, and Karima Tamsamani.

Conflicts of Interest: The authors declare no conflict of interest.

References

1. Campillo, C.; Fortes, R.; del Henar Prieto, M. *Solar Radiation Effect on Crop Production*; Centro de Investigación finca la Orden-Valdesequera: Badajoz, Spain, 2012. [CrossRef]

2. Grancher-Varlet, C.; Bonhomme, R.; Sinoquet, H. *Crop Structure and Light Microclimate Characterization and Applications, Éditions INRA*; Institute National de la Recherche Agronomique: Paris, France, 1993; p. 518.
3. de Souza, D.F.; da Silva, P.P.F.; Fontenele, L.F.A.; Barbosa, G.D.; de Oliveira Jesus, M. Efficiency, quality, and environmental impacts: A comparative study of residential artificial lighting. *Energy Rep.* **2019**, *5*. [CrossRef]
4. Bergstrand, K.J.; Schüssler, H.K. Growth, development and photosynthesis of some horticultural plants as affected by different supplementary lighting technologies. *Eur. J. Hortic. Sci.* **2013**, *78*, 119–125.
5. Watanabe, H. Light-Controlled Plant Cultivation System in Japan—Development of a Vegetable Factory Using LEDs as a Light Source for Plants. In Proceedings of the VI International Symposium on Light in Horticulture, Tsukuba, Japan, 15–19 November 2009; Goto, E., Hikosaka, S., Eds.; International Society for Horticultural Science: Leuven, Belgium, 2011; Volume 907. [CrossRef]
6. Barta, D.J.; Tibbitts, T.W.; Bula, R.J.; Morrow, R.C. Evaluation of light emitting diode characteristics for a space-based plant irradiation source. *Adv. Space Res.* **1992**, *12*. [CrossRef]
7. Bula, R.J.; Morrow, R.C.; Tibbitts, T.W.; Barta, D.J.; Ignatius, R.W.; Martin, T.S. Light-emitting diodes as a radiation source for plants. *HortSci. A Publ. Am. Soc. Hortic. Sci.* **1991**, *26*. [CrossRef]
8. Heffernan, W.; Frater, L.; Watson, N. LED replacement for fluorescent tube lighting. In Proceedings of the IEEE Australasian Universities Power Engineering Conference, Perth, WA, Australia, 9–12 December 2007; pp. 1–6. [CrossRef]
9. Wei, A.C.; Huang, Y.J.; Huang, B.L.; Sze, J.R. Integration of optical and thermal models for organic light-emitting diodes. *Electronics* **2019**, *8*, 17. [CrossRef]
10. Wei, A.C.; Sze, J.R. Modeling OLED lighting using Monte Carlo ray tracing and rigorous coupling wave analyses. *Opt. Commun.* **2016**, *380*. [CrossRef]
11. Doulos, L.T.; Sioutis, I.; Tsangrassoulis, A.; Canale, L.; Faidas, K. Revision of threshold luminance levels in tunnels aiming to minimize energy consumption at no cost: Methodology and case studies. *Energies* **2020**, *13*, 1707. [CrossRef]
12. Grigoropoulos, C.J.; Doulos, L.T.; Zerefos, S.C.; Tsangrassoulis, A.; Bhusal, P. Estimating the benefits of increasing the recycling rate of lamps from the domestic sector: Methodology, opportunities and case study. *Waste Manag.* **2020**, *101*. [CrossRef] [PubMed]
13. Singh, D.; Basu, C.; Meinhardt-Wollweber, M.; Roth, B. LEDs for energy efficient greenhouse lighting. *Renew. Sustain. Energy Rev.* **2015**, *49*, 139–147. [CrossRef]
14. Sharma, A. *Horticulture LED Lighting Market Size, Share and Trends Analysis Report 2018–2025*; Value Market Research; 2018. Available online: https://www.valuemarketresearch.com/report/horticulture-led-lighting-market (accessed on 28 November 2020).
15. Lukyanov, A.; Donskoy, D.; Vernezi, M. Simulation, identification and dynamic control of the luminaire of the synthesized spectrum. In *MATEC Web of Conferences*; EDP Sciences: Ulis, France, 2018; Volume 226. Available online: https://www.matec-conferences.org/articles/matecconf/pdf/2018/85/matecconf_dts2018_02030.pdf (accessed on 1 January 2021)
16. Wei, A.C.; Lo, S.C.; Lee, J.Y.; Yeh, H.Y. Cost-Effective Light-Mixing Module for Solar-Lighting System Appended with Auxiliary RGBW Light-Emitting Diodes. *J. Sol. Energy Eng. Trans. ASME* **2017**, *139*. [CrossRef]
17. Tamulaitis, G. High-power LEDs for plant cultivation. *Int. Soc. Opt. Photonics* **2004**. [CrossRef]
18. Nicole, C.; Charalambous, F.; Martinakos, S.; van de Voort, S.; Li, Z.; Verhoog, M.; Krijn, M. Lettuce growth and quality optimization in a plant factory. *Acta Hortic.* **2016**, 231–238. [CrossRef]
19. Mao, R.; Guo, S. Performance of the mixed LED light quality on the growth and energy efficiency of Arthrospira platensis. *Appl. Microbiol. Biotechnol.* **2018**, *102*. [CrossRef] [PubMed]
20. Oh, J.H.; Kang, H.; Park, H.K.; Do, Y.R. *RSC Advances Performance and Vision-Friendly Quality of Multi-Package Purplish White LED Lighting*; Royal Society of Chemistry: London, UK, 2015; pp. 21745–21754. [CrossRef]
21. Ahlman, L.; Bånkestad, D.; Wik, T. Using chlorophyll a fluorescence gains to optimize LED light spectrum for short term photosynthesis. *Comput. Electron. Agric.* **2017**, *142*, 224–234. [CrossRef]
22. van Iersel, M.W. Optimizing LED Lighting in Controlled Environment Agriculture. In *Light Emitting Diodes for Agriculture*; Springer: Singapore, 2017; pp. 59–80. [CrossRef]
23. Loconsole, D.; Cocetta, G.; Santoro, P.; Ferrante, A. Optimization of LED Lighting and Quality Evaluation of Romaine Lettuce Grown in an Innovative Indoor Cultivation System. *Sustainability* **2019**, *11*, 841. [CrossRef]
24. Avercheva, O.V.; Berkovich, Y.A.; Konovalova, I.O.; Radchenko, S.G.; Lapach, S.N.; Bassarskaya, E.M.; Kochetova, G.V.; Zhigalova, T.V.; Yakovleva, O.S.; Tarakanov, I.G. Life Sciences in Space Research Optimizing LED lighting for space plant growth unit: Joint effects of photon flux density, red to white ratios and intermittent light pulses. *Life Sci. Space Res.* **2016**, *11*, 29–42. [CrossRef]
25. He, F.; Zeng, L.; Li, D.; Ren, Z. Study of LED array fill light based on parallel particle swarm optimization in greenhouse planting. *Inf. Process. Agric.* **2019**, *6*, 73–80. [CrossRef]
26. Zielinska-Dabkowska, K.M.; Hartmann, J.; Sigillo, C. LED light sources and their complex set-up for visually and biologically effective illumination for ornamental indoor plants. *Sustainability* **2019**, *11*, 2642. [CrossRef]
27. Prikupets, L. Photobiological researches—A way to optimize LED'S plant lighting. In Proceedings of the 29th CIE SESSION, Washington, DC, USA, 17–19 June 2019. [CrossRef]
28. McCree, K.J. The action spectrum, absorbance and quantum yield of photosynthesis in crop plants. *Agric. Meteorol.* **1971**, *9*, 191–216. [CrossRef]
29. Inada, K. Action spectra for photosynthesis in higher plants. *Plant Cell Physiol.* **1976**, *17*, 355–365.

30. Wu, B.S.; Rufyikiri, A.S.; Orsat, V.; Lefsrud, M.G. Re-interpreting the photosynthetically action radiation (PAR) curve in plants. *Plant Sci.* **2019**, *289*. [CrossRef]
31. Da Costa, G.J.; Cuello, J.L. The phytometric system: A new concept of light measurement for plants. *J. Illum. Eng. Soc.* **2004**, *33*, 34–42. [CrossRef]
32. Mõttus, M.; Sulev, M.; Frederic, B.; Lopez-Lozano, R.; Noorma, A. *Photosynthetically Active Radiation: Measurement and Modeling*; Springer Science: New York, NY, USA, 2011; pp. 7970–8000. [CrossRef]
33. Gallo, K.; Daughtry, C. Techniques for measuring intercepted and absorbed Photosynthetically Active Radiation in Corn Canopies 1. *Agron. J.* **1986**, *78*, 752–756. [CrossRef]
34. Hershey, D.R. Plant Light Measurement & Calculations. *Am. Biol. Teach.* **1991**, *53*. [CrossRef]
35. McCree, K.J. Test of current definitions of photosynthetically active radiation against leaf photosynthesis data. *Agric. Meteorol.* **1972**, *10*, 443–453. [CrossRef]
36. Lopez, F.; Barclay, G. Plant anatomy and physiology. In *Pharmacognosy*; Elsevier: Amsterdam, The Netherlands, 2017; pp. 45–60.
37. Smith, J.H.C.; French, C.S. The Major and Accessory Pigments in Photosynthesis. *Annu. Rev. Plant Physiol.* **1963**, *14*. [CrossRef]
38. Kong, Y.; Schiestel, K.; Zheng, Y. *Does "Blue" Light Invariably Cause Plant Compactness? Not Really: A Comparison with Red Light in Four Bedding Plant Species during the Transplant Stage*; International Society for Horticultural Science: Leuven, Belgium; Angers, France, 2020; Volume 1296. [CrossRef]
39. Kong, Y.; Zheng, Y. Growth and morphology responses to narrow-band blue light and its co-action with low-level UVB or green light: A comparison with red light in four microgreen species. *Environ. Exp. Bot.* **2020**, *178*. [CrossRef]
40. Kong, Y.; Kamath, D.; Zheng, Y. Blue-light-promoted elongation and flowering are not artifacts from 24-h lighting: A comparison with red light in four bedding plant species. *Acta Hortic.* **2020**, *1296*. [CrossRef]
41. Kong, Y.; Schiestel, K.; Zheng, Y. Blue light associated with low phytochrome activity can promote flowering: A comparison with red light in four bedding plant species. *Acta Hortic.* **2020**, *1296*. [CrossRef]
42. Goto, E. Effects of Light Quality on Growth of Crop Plants under Artificial Lighting. *Environ. Control Biol.* **2003**, *41*. [CrossRef]
43. Yanagi, T.; Okamoto, K.; Takita, S. *Effects of Blue, Red, and Blue/Red Lights of Two Different PPF Levels on Growth and Morphogenesis of Lettuce Plants*; International Society for Horticultural Science: Leuven, Belgium; Narita, Japan, 1996; Volume 440. [CrossRef]
44. Lopez-Figueroa, F.; Niell, F.X. Red-light and blue-light photoreceptors controlling chlorophyll a synthesis in the red alga Porphyra umbilicalis and in the green alga Ulva rigida. *Physiol. Plant.* **1989**, *76*. [CrossRef]
45. Chen, X.L.; Yang, Q.C.; Song, W.P.; Wang, L.C.; Guo, W.Z.; Xue, X.Z. Growth and nutritional properties of lettuce affected by different alternating intervals of red and blue LED irradiation. *Sci. Hortic.* **2017**, *223*. [CrossRef]
46. Yerima, J.B.; Esther, M.A.; Madugu, J.S.; Muwa, N.S.; Timothy, S.A. The effect of Light Color (wavelength) and Intensity on Vegetable Roselle (Hibiscus Sabdariffa) growth. *Sch. J. Sci. Res. Essay* **2012**, *12*, 19–29.
47. Niangoran, N.U.; Canale, L.; Tian, F.; Haba, T.C.; Zissis, G. Optimal spectrum modeling calculation with light emitting diodes set based on relative quantum efficiency. *Acta Hortic.* **2019**, *1242*. [CrossRef]
48. Driel, W.D.V.; Fan, X.J. *Solid State Lighting Reliability: Components to Systems*; Springer Nature Switzerland AG: Cham, Switzerland, 2013. [CrossRef]
49. Multicomp THEM-CLRX (RED) Datasheet. Available online: https://datasheet.octopart.com/THEM-CLRX-%28RED%29-Multicomp-datasheet-66420695.pdf (accessed on 19 March 2021).
50. Multicomp THEM-CLGX(520535) Datasheet. Available online: https://datasheet.octopart.com/THEM-CLGX%28520535%29-Multicomp-datasheet-66420694.pdf (accessed on 19 March 2021).
51. Multicomp THEM-CLAX(AMBER) Datasheet. Available online: https://datasheet.octopart.com/THEM-CLAX%28AMBER%29-Multicomp-datasheet-66420692.pdf (accessed on 19 March 2021).
52. Multicomp THEM-CLBX(460-470) Datasheet. Available online: https://datasheet.octopart.com/THEM-CLBX%28460-470%29-Multicomp-datasheet-66420693.pdf (accessed on 19 March 2021).
53. Golden DRAGON®, LW W5SM | OSRAM Opto Semiconductors. Available online: https://www.osram.com/ecat/Golden%20DRAGON%C2%AE%20LD%20W5SM/com/en/class_pim_web_catalog_103489/prd_pim_device_2190689/ (accessed on 19 March 2021).
54. OSLON® SSL 150, GH CSHPM1.24 | OSRAM Opto Semiconductors. Available online: https://www.osram.com/ecat/OSLON%C2%AE%20SSL%20150%20GH%20CSHPM1.24/com/en/class_pim_web_catalog_103489/prd_pim_device_2402537/ (accessed on 19 March 2021).
55. Golden DRAGON® Plus, LH W5AM | OSRAM Opto Semiconductors. Available online: https://www.osram.com/ecat/Golden%20DRAGON%C2%AE%20Plus%20LH%20W5AM/com/en/class_pim_web_catalog_103489/prd_pim_device_2402623/$?$query=%20LH%20W5AM%20680&page=1&configure%5BhitsPerPage%5D=18&configure%5BclickAnalytics%5D=true (accessed on 19 March 2021).
56. Golden DRAGON® Plus, LA W5AM | OSRAM Opto Semiconductors. Available online: https://www.osram.com/ecat/Golden%20DRAGON%C2%AE%20Plus%20LA%20W5AM/com/en/class_pim_web_catalog_103489/prd_pim_device_2402620/ (accessed on 19 March 2021).
57. Bridgelux ES Rectangle Array Series. Available online: https://www.bridgelux.com/sites/default/files/resource_media/DS23-Bridgelux-ES-Star-Array-Data-Sheet1.pdf (accessed on 19 March 2021).

58. Bodrogi, P.; Guo, X.; Stojanovic, D.; Fischer, S.; Khanh, T.Q. Observer preference for perceived illumination chromaticity. *Color Res. Appl.* **2018**, *43*, 506–516. [CrossRef]
59. Bodrogi, P.; Vinh, Q.T.; Khanh, T.Q. Correlations among lighting quality metrics for interior lighting. *Light. Res. Technol.* **2019**, *51*. [CrossRef]
60. Bodrogi, P.; Carella, D.; Khanh, T.Q. Weighting the relevance of the different colours in subjective assessments of colour preference. *Light Eng.* **2020**, *28*. [CrossRef]
61. Kuo, Y.K.; Chang, J.; Horng, K.; Huang, Y.; Chang, Y.; Huang, H. *Temperature-Dependent Optical Properties of InGaN Semiconductor Materials: Experimental and Numerical Studies*; SPIE, Photonics Taiwan: Taipei, Taiwan, 2000; Volume 4078. [CrossRef]
62. Uchida, Y. Lighting theory and luminous characteristics of white light-emitting diodes. *Opt. Eng.* **2005**, *44*. [CrossRef]
63. Ohno, Y. Spectral design considerations for white LED color rendering. *Opt. Eng.* **2005**, *44*. [CrossRef]
64. Man, K.; Ashdown, I. Accurate Colorimetric Feedback for RGB LED Clusters. In Proceedings of the SPIE OPTICS + PHOTONICS, San Diego, CA, USA, 13–17 August 2006; Volume 6337. [CrossRef]
65. Chien, M.C.; Tien, C.H. Multispectral mixing scheme for LED clusters with extended operational temperature window. *Opt. Express* **2012**, *20*. [CrossRef]
66. Chou, H.Y.; Yang, T.H. Dependence of emission spectra of LEDs upon junction temperature and driving current. *J. Light Vis. Environ.* **2008**, *32*, 183–186. [CrossRef]
67. Reifegerste, F.; Lienig, J. Modelling of the temperature and current dependence of LED spectra. *J. Light Vis. Environ.* **2008**, *32*. [CrossRef]
68. Heimpold, T.; Reifegerste, F.; Drechsel, S.; Lienig, J. Spectral Deviation: A New Parameter for Efficient Design of High Quality Tuneable White Lighting. *J. Sci. Technol. Light.* **2018**, *41*. [CrossRef]
69. Heimpold, T.; Reifegerste, F.; Drechsel, S.; Lienig, J. LED for hyperspectral imaging—A new selection method. *Biomed. Tech.* **2018**, *63*. [CrossRef]
70. Bachouch, L. (Carthage University, Tunis, Tunisia); Reifegerste, F. (Technical University Dresden Institute for Precision Engineering and Electronic Design, Dresden, Germany). Personal communication, December 2020.
71. Keppens, A.; Ryckaert, W.R.; Deconinck, G.; Hanselaer, P. Modeling High Power Light-Emitting Diode Spectra and Their Variation with Junction Temperature. *AIP J. Appl. Phys.* **2010**, *108*. [CrossRef]
72. Vinh, Q.T.; Khanh, T.Q.; Ganev, H.; Wagner, M. Measurement and Modeling of the LED Light Source. *LED Light. Technol. Percept.* **2015**, 167–170. [CrossRef]
73. Ohtani, K.; Tanizaki, H. Exact Distributions of R^2 and Adjusted R^2 in a Linear Regression Model with Multivariate t Error Terms. *J. Jpn. Stat. Soc.* **2004**, *34*. [CrossRef]
74. Kennedy, J.; Eberhart, R. Particle swarm optimization. In Proceedings of ICNN'95—International Conference on Neural Networks, Perth, WA, Australia, 27 November–1 December 1995; Volume 4, pp. 1942–1948. [CrossRef]
75. Tian, F. Étude et Optimisation des Systémes D'éclairage pour la Croissance des Plantes en Milieu Contrôlé. Ph.D. Thesis, Université de Toulouse, Toulouse, France, 2016. Available online: http://thesesups.ups-tlse.fr/3374/ (accessed on 1 July 2020).
76. Bachouch, L.; Bouslimi, L.; El Amraoui, L. Power losses minimization in the SEPIC DC-DC converter using Particle Swarm Optimization technique (PSO). In Proceedings of the 19th International Conference on Sciences and Techniques of Automatic Control and Computer Engineering, Sousse, Tunisia, 24–26 March 2019. [CrossRef]
77. Bouslimi, L.; Bachouch, L.; El Amraoui, L.; Zissis, G. Design and optimization of a DC-DC converter for LEDs lighting applications. In Proceedings of the 13th International Conference on Power Electronics and Drive Systems (PEDS), Toulouse, France, 9–12 July 2019. [CrossRef]
78. Bachouch, L.; Dupuis, P.; Sewraj, N.; Canale, L.; Zissis, G.; Bouslimi, L.; El Amraoui, L. Tunable multiple-LEDs combination spectrum for plants based on McCree PAR spectrum. In Proceedings of the—2020 IEEE International Conference on Environment and Electrical Engineering and 2020 IEEE Industrial and Commercial Power Systems Europe, Madrid, Spain, 9–12 June 2020. [CrossRef]